Comparison of diffraction-enhanced computed tomography and monochromatic synchrotron radiation computed tomography of human trabecular bone

2009 Phys. Med. Biol. 54 6123

(http://iopscience.iop.org/0031-9155/54/20/006)

IOP PUBLISHING PHYSICS IN MEDICINE AND BIOLOGY

Phys. Med. Biol. **54** (2009) 6123–6133 doi:10.1088/0031-9155/54/20/006

Comparison of diffraction-enhanced computed tomography and monochromatic synchrotron radiation computed tomography of human trabecular bone

D M Connor[1,2,5], H D Hallen[2], D S Lalush[3], D R Sumner[4] and Z Zhong[1]

[1] Department of Biomedical Engineering, Biomedical Research Imaging Center, University of North Carolina at Chapel Hill, 4030 Bondurant Hall, CB 7000, Chapel Hill, NC 27599, USA
[2] Department of Physics, North Carolina State University, 2700 Stinson Drive, Box 8202, Raleigh, NC 27695, USA
[3] Department of Biomedical Engineering, North Carolina State University, 2700 Stinson Dr, Box 7115, Raleigh, NC 27695, USA
[4] Department of Anatomy and Cell Biology, Rush University Medical Center, 600 South Paulina, Suite 507, Chicago, IL 60612, USA

E-mail: connord@bnl.gov

Received 12 February 2009, in final form 24 August 2009
Published 24 September 2009
Online at stacks.iop.org/PMB/54/6123

Abstract

Diffraction-enhanced imaging (DEI) is an x-ray-based medical imaging modality that, when used in tomography mode (DECT), can generate a three-dimensional map of both the apparent absorption coefficient and the out-of-plane gradient of the index of refraction of the sample. DECT is known to have contrast gains over monochromatic synchrotron radiation CT (SRCT) for soft tissue structures. The goal of this experiment was to compare contrast-to-noise ratio (CNR) and resolution in images of human trabecular bone acquired using SRCT with images acquired using DECT. All images were acquired at the National Synchrotron Light Source (Upton, NY, USA) at beamline X15 A at an x-ray energy of 40 keV and the silicon [3 3 3] reflection. SRCT, apparent absorption DECT and refraction DECT slice images of the trabecular bone were created. The apparent absorption DECT images have significantly higher spatial resolution and CNR than the corresponding SRCT images. Thus, DECT will prove to be a useful tool for imaging applications in which high contrast and high spatial resolution are required for both soft tissue features and bone.

1. Introduction

Diffraction-enhanced imaging, alternately referred to as analyzer-based imaging (ABI) (Bravin 2003, Coan *et al* 2005, Davis 1996, Davis *et al* 1995, Forster *et al* 1980, Ingal and Beliaevskaya

[5] Author to whom any correspondence should be addressed.

1997, Pagot *et al* 2003, Pavlov *et al* 2004), in computed tomography mode (DECT) has been shown to have significant contrast gains over comparably obtained monochromatic synchrotron radiation computed tomography (SRCT) for mammography (Fiedler *et al* 2004, Keyriläinen *et al* 2008), a soft tissue imaging application. The goal of this experiment was to compare the contrast-to-noise ratio (CNR) and spatial resolution for images of human trabecular bone, a hard tissue imaging application, acquired using monochromatic synchrotron radiation computed tomography (SRCT) with those acquired using diffraction-enhanced computed tomography (DECT).

2. Background

2.1. Assessing trabecular structure

Osteoporosis is a disease of the bone that leads to a reduction in bone mass and a decrease in bone strength. It most severely affects trabecular bone—the spicular scaffolding present at the end of long bones and in vertebrae—where osteoporotic fractures often occur (Keaveny *et al* 2001). Correlations have been drawn between the biomechanical strength of trabecular bone and certain trabecular measures (Ulrich *et al* 1999, Keaveny *et al* 2001, Link *et al* 1999). The most common of these morphological parameters are the average spacing between the trabeculae (Tb.Sp), the average trabecular thickness (Tb.Th), the number of trabeculae in a region (Tb.N) and the ratio of the bone volume to total volume in a region of trabecular bone (BV/TV).

Imaging methods that can accurately determine bone strength are essential to diagnose osteoporosis, to evaluate bone deterioration and to assess the effectiveness of treatment methods. High-resolution, micro-computed tomography (microCT) has been shown to be an effective method to predict bone strength and to assess trabecular structure. When measuring these parameters with microCT, the data must first be thresholded—a process whereby each voxel is marked as being either bone or marrow—then proprietary software is used to determine the morphological parameters. The spatial resolution and contrast-to-noise ratio (CNR) of the imaging system affect the ability to accurately measure these parameters (Kothari *et al* 1998, Muller *et al* 1996).

2.2. Diffraction-enhanced imaging experiments

Though still in its early stages of development and testing as a medical imaging modality, diffraction-enhanced imaging (DEI), sometimes referred to as analyzer-based imaging (ABI), has shown much promise in several different areas of medical imaging. The largest thrust has been toward using DEI for mammography where it has shown contrast advantages over radiography for both planar (Hasnah *et al* 2002, 2005, Kiss *et al* 2004, Pisano *et al* 2000, Chapman *et al* 1996, 1997) and CT imaging (Fiedler *et al* 2004, Keyriläinen *et al* 2008, Arfelli *et al* 2000, Bravin *et al* 2007). DEI has also been shown to have contrast advantages over standard radiography for the imaging of soft tissue in joints (Li *et al* 2004, Majumdar *et al* 2004, Mollenhauer *et al* 2002, Muehleman *et al* 2002, 2003, 2004a, 2004b, Wagner *et al* 2004). Other studies have been done for testing DEI's effectiveness in imaging kidneys (Gang *et al* 2004), the brain (Mannan *et al* 2004, Connor *et al* 2007, 2009), the thyroid (Rocha *et al* 2004) and bone (Connor *et al* 2005, 2006, Wagner *et al* 2006, Majumdar *et al* 2004). Of these experiments, three are particularly pertinent to this study. Kiss *et al* (2004) have shown that DEI, because of additional extinction contrast, has considerable contrast gains over standard radiography for the imaging of calcifications in breast tissue. This is pertinent because the

calcifications are dense and scattered and lying in a bed of soft tissue, not unlike trabecular bone (dense and scattering) lying in a bed of marrow. Fiedler *et al* (2004) were the first to report on DECT of biological tissue. They showed that DECT achieves appreciable contrast gains over SRCT in the imaging of invasive lobular carcinoma in adipose tissue in the breast. In a prior study, the author (DMC) has shown that bone has measurable ultra-small angle scattering (USAXS) (Connor *et al* 2005).

2.3. DEI description

DEI is a type of phase contrast imaging in which physical properties of an analyzer crystal are exploited to reject or selectively accept scattered x-rays and to retrieve refraction information from a sample (Chapman *et al* 1996, 1997, Zhong *et al* 2000, Dilmanian *et al* 2000, Wernick *et al* 2003, Oltulu *et al* 2003, Pagot *et al* 2003). For x-ray energies that are usable in medical imaging (20–60 keV), an analyzer crystal has a reflectivity profile, called a rocking curve, with a width on the order of microradians (Zachariasen 1945). Any transmitted x-rays that deviate by more than a few microradians from the analyzer crystal's Bragg peak will not be reflected by the analyzer crystal. This means that all small-angle x-ray scattering (SAXS; on the order of milliradians) and all but a very narrow range of ultra-small angle x-ray scattering (USAXS; on the order of microradians) are rejected by the analyzer crystal. This rejection of scattered x-rays leads to additional contrast, called extinction contrast, in the DEI projection image.

Several different forms of DEI are now being used. In all DEI forms, the analyzer crystal is tilted to positions relative to its peak reflectivity position. For this study, the two-image DEI method, previously described for both planar imaging (Chapman *et al* 1997) and CT (Dilmanian *et al* 2000), is used. In the two-image method, the analyzer crystal is tilted to the high-angle and low-angle sides of the rocking curve that correspond to half the peak reflectivity. By combining these high-angle and low-angle projection images, an apparent absorption image and a refraction image can be created. The apparent absorption image should appear similar to a standard radiography image, but with additional extinction contrast. Scattering materials (such as bone) will appear to be more absorbing in the apparent absorption image than they would in a standard radiograph. As with SRCT, the apparent absorption images are used to create a three-dimensional map of the absorption coefficient in the sample. In tomography mode, the refraction projection images are used to create a three-dimensional map of the out-of-plane gradient of the index of refraction within the sample (Dilmanian *et al* 2000), so image contrast is related to the change in the index of refraction along the vertical direction.

Because trabecular bone has a structure on a scale that can be visualized using the current diffraction-enhanced imaging (DEI) system and its structure both refracts and scatters, it is a good test of two-image DEI.

3. Materials and methods

Formalin-fixed human tibial trabecular bone samples were obtained from the Gift of Hope Organ and Tissue Donor Network with Institutional Review Board (IRB) approval. The samples were cut into cylindrical cores measuring about 0.8 cm in diameter and about 1 cm in height and fixed to a small metal platform using epoxy. The metal platform was placed in a water-filled acrylic cylinder that was attached to a rotating sample stage which was attached to a scanning stage.

The data were obtained at the National Synchrotron Light Source (NSLS) beamline X15A. A diagram of the experimental setup at X15A is included in figure 1. Two major changes have been made to the original DEI setup (Zhong *et al* 2000): the rotation stage has

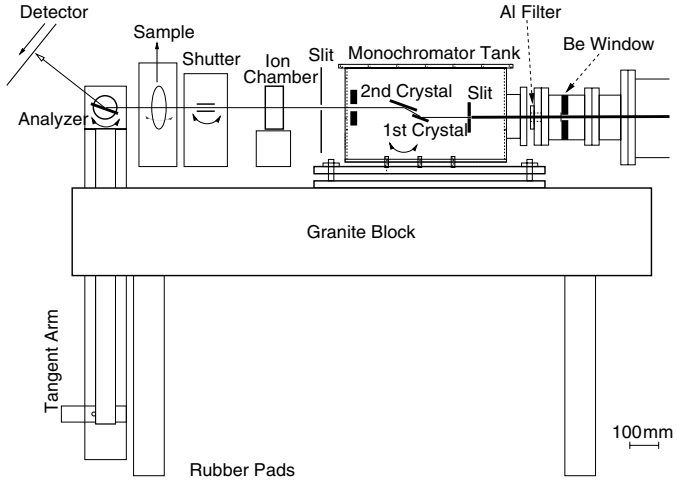

Figure 1. Diagram of the experimental setup at Beamline X15A at the National Synchrotron Light Source, Upton, NY, USA.

been added to the scanning stage to allow for CT and the imaging plate has been replaced by a Rad-icon Shad-o-Box^{TM} 2048 X-Ray Camera which generates 2048 by 1024 images with a 50 μm by 50 μm pixel size. This study was done with future clinical applications in mind; a detector with a 50 μm detector element is on the lower end for a clinically relevant CT resolution. The double-crystal monochromator and analyzer crystal of the DEI system were tuned to 40 keV using the silicon [3 3 3] reflection. To create a full DECT image set, 720 projection images were taken rotating the sample in 0.5° increments with the analyzer crystal tuned to +0.8 μrad and then -0.8 μrad with respect to the Bragg peak. The exposure time for each projection image was 1 s. Since there was a delay of about 1 s between each of the images, the total acquisition time for each 720 image set was approximately 20 min. Prior to CT reconstruction, the projection images were combined to form refraction and apparent absorption images using the DEI equations of Chapman *et al* (1997).

The SRCT images were acquired as described above with 720 projection images in 0.5° increments and a 1 s acquisition time per image, but with the analyzer crystal removed. Apparent absorption DECT, refraction DECT and SRCT reconstructions of the trabecular bone were created using filtered back-projection with a Shepp–Logan filter and ring artifact correction using a modification of IDL (ITT Visual Information Systems, Boulder, CO) code developed by Rivers (1998). These 2D slices were then exported from IDL as 8-bit TIFF files. The files were imported to Photoshop where they were histogram- and gamma-corrected.

As a measure of system resolution, line profiles were taken through the smallest trabecular features that were perceptible in the apparent absorption DECT, refraction DECT and SRCT slices. The line profiles from both the apparent absorption DECT and SRCT profiles were fit to a Gaussian and the FWHM from each was recorded. All three line profiles were also used to determine an average CNR for these small features in bone. For the apparent absorption and SR profiles, the CNR was determined using

$$\mathrm{CNR} = \frac{\mu_{\max} - \mu_{\min}}{\sigma_{\mathrm{back}}}, \tag{1}$$

where σ_{back} is the standard deviation in a 30 by 30 pixel section of the slice containing only water, and $\mu_{\max}$ and $\mu_{\min}$ are the maximum and minimum values, respectively, of the absorption coefficient along the line profile. For the refraction profiles, the CNR was determined using

$$\text{CNR}_{\text{refr}} = \frac{\left(\frac{\partial n}{\partial z}\right)_{\max} - \left(\frac{\partial n}{\partial z}\right)_{\min}}{\sigma_{\text{back}}}, \tag{2}$$

where σ_{back} is the standard deviation in a 30 by 30 pixel section of the slice containing only water, and $\left(\frac{\partial n}{\partial z}\right)_{\max}$ and $\left(\frac{\partial n}{\partial z}\right)_{\min}$ are the maximum and minimum values, respectively, of the z-gradient of the index of refraction as measured along the line profile. The apparent absorption and refraction gains, defined as the ratio of the CNR from the DECT slices to the CNR from the SRCT slices ($\text{CNR}_{\text{appab}}/\text{CNR}_{\text{SR}}$ and $\text{CNR}_{\text{refr}}/\text{CNR}_{\text{SR}}$), were then recorded.

In order to get a more accurate measure of the true trabecular sizes, high-resolution images were obtained at beamline X15A of the NSLS using an x-Ray Image VHR 1:1 detector (Photonic Science Limited, UK) with a 9 μm pixel size. The system optics were configured to the 23 keV, silicon [1 1 1] reflection. The 23 keV, [1 1 1] reflection was chosen because of its optical stability (due to its wide rocking curve), scatter-rejection properties and relatively low sensitivity to refraction. With the analyzer crystal set to the peak position, images were taken in 0.18° increments over a range of 360° ($n_{\text{images}} = 2000$) with an exposure time of 0.4 s per image. The images were reconstructed in IDL. After reconstruction, five of the resulting slice images were opened in ImageJ (National Institutes of Health, Bethesda, MD, USA). Using the line measurement tool in ImageJ, the thickness of the trabeculae was measured at 736 different image locations.

4. Results

Four SRCT and apparent absorption DECT slice images of corresponding sections of bone are displayed in figure 2. Qualitatively, the apparent absorption image appears sharper than the radiograph image. The SR image shows more connectedness between trabecular structures than the apparent absorption slice does.

Figure 3 includes slice image comparisons between corresponding apparent absorption and refraction slice images. The trabecular structures that can be seen as a dot in the apparent absorption image can be seen at the same location in the refraction image, but as a white and black dot surrounded by gray. Because the refraction slice presents a measure of the out-of-plane gradient of the index of refraction, the refraction image contains information on the orientation of the trabecular structures within the slice.

A high-resolution peak DECT slice image is displayed in figure 4(a). The average thickness of the trabeculae is 90 ± 50 μm and the distribution of trabecular thicknesses is plotted in figure 4(b). Though there are still errors in the trabecular size due to the partial volume effect, the trabecular thickness as measured by this high-resolution CT is considered here to be the true thickness of the trabeculae.

The average FWHM for the line profiles in the apparent absorption DECT slice was 160 ± 20 μm and for the SRCT slice was 200 ± 40 μm using a total of 18 line profiles from each image set. The median 1-sigma error estimate for the FWHM measurements from the individual line profiles is 12 μm for the apparent absorption CT and 17 μm for the SRCT image. The measured sizes represent 180% ± 60% and 220% ± 60% of the true trabecular sizes for the apparent absorption DECT and the SRCT measurements, respectively. As expected, because of the greater relative partial volume effect for the 50 μm pixel size compared to the 9 μm pixel size, both the apparent absorption DECT and the SRCT images yielded significantly larger average trabecular size than the high-resolution CT image did.

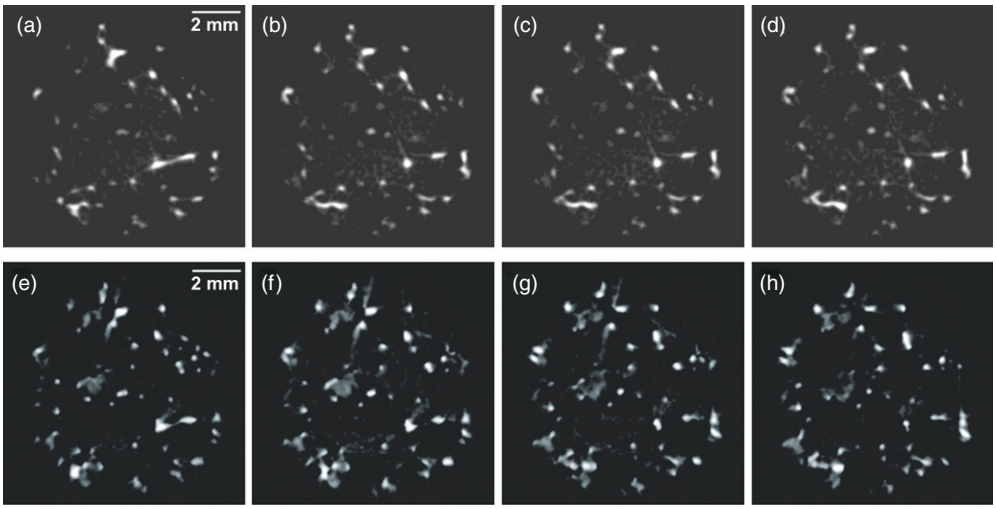

Figure 2. Example slice images of trabecular bone. Images (a)–(d) are consecutive slices from monochromatic synchrotron radiation computed tomography. Images (e)–(h) are from apparent absorption diffractionenhanced computed tomography.

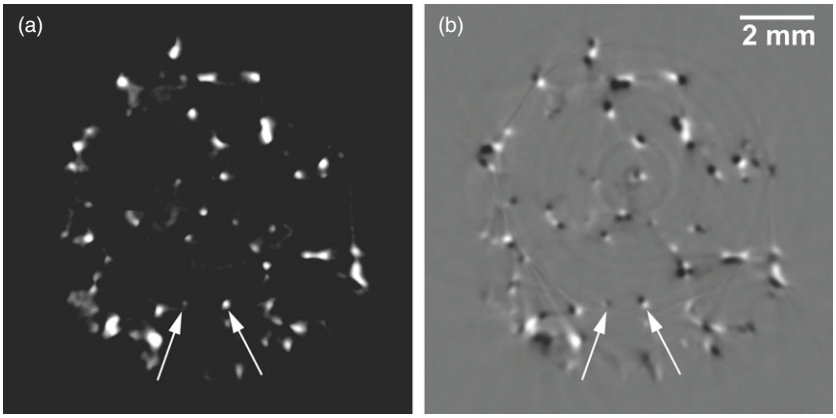

Figure 3. Comparison slice images of trabecular bone from (a) apparent absorption DECT and (b) refraction DECT.

Line profile plots from a corresponding feature in an SRCT slice and an apparent absorption and refraction DECT slice are shown in figures 5(a), (c) and (e), respectively. The region of each image used to create the line profile is circled in the corresponding SRCT, apparent absorption DECT or refraction DECT image (figures 5(b), (d) and (f)). A paired *t*-test was performed with the alternative hypothesis that the true mean $\mathrm{FWHM}_{\mathrm{appabDECT}}$ was less than the true mean $\mathrm{FWHM}_{\mathrm{SRCT}}$ and a confidence interval of 99%. The paired *t*-test showed the difference between the feature widths to be statistically significant ($p < 0.001$). The narrower FWHM for the apparent absorption DECT images suggests that it offers higher resolution than the SRCT image. The average apparent absorption CNR gain of 2.2 ± 0.7 compared to SRCT was found.

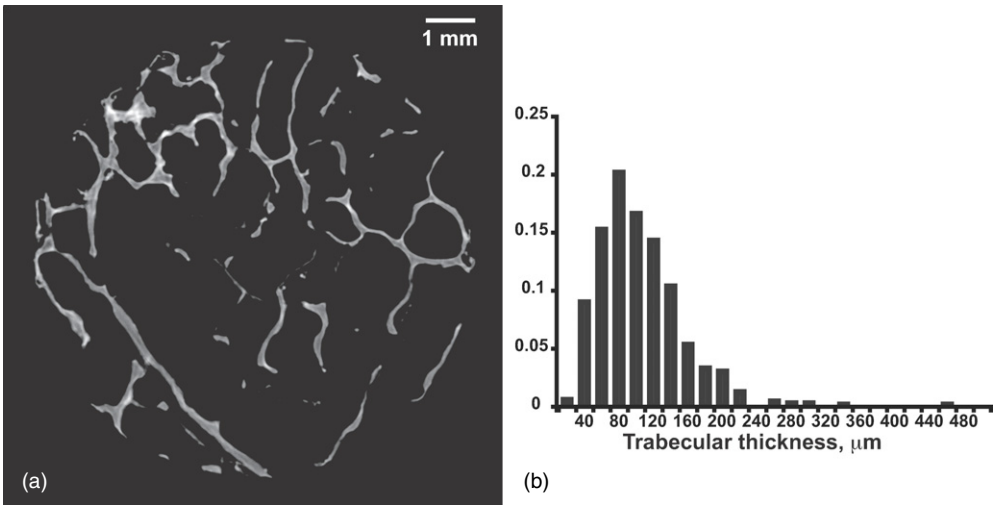

Figure 4. Example high-resolution peak DECT slice image with corresponding trabecular size distribution. DECT slice image (a) was acquired at the peak of the 23 keV, [1 1 1] rocking curve with a 9 μm pixel size detector. (b) The normalized plot of the size distribution of the trabulae.

A paired *t*-test was performed with the alternative hypothesis that the true mean $\mathrm{CNR}_{\mathrm{appabDECT}}$ was greater than the true mean $\mathrm{CNR}_{\mathrm{SRCT}}$ and a confidence interval of 99%. The paired *t*-test showed the difference between the CNR values to be statistically significant ($p < 0.0001$), so the CNR gain was statistically significant. A gain in CNR means that the bone region of the apparent absorption DECT slice stands out more against the background (surrounding water) than it does in an SRCT slice. An average refraction CNR gain of 3.7 ± 1.4 compared to SRCT was found. A paired *t*-test was performed with the alternative hypothesis that the true mean $\mathrm{CNR}_{\mathrm{refrDECT}}$ was greater than the true mean $\mathrm{CNR}_{\mathrm{SRCT}}$ and a confidence interval of 99%. The paired *t*-test showed the difference between the CNR values to be statistically significant ($p < 0.0001$), so the CNR gain of refraction DECT over SRCT was statistically significant.

5. Discussion

In this investigation of DECT of trabecular bone, we have found that apparent absorption DECT has significant gains in both resolution and CNR over monochromatic synchrotron radiation CT for imaging trabecular bone structure. Because measures for the morphological parameters in trabecular bone are affected by system resolution, an increase in system resolution suggests that the DECT could produce more accurate morphological parameters than SRCT. The gain in both resolution and contrast, for a given radiation dose, x-ray energy and detector resolution, will allow for thresholding of the data that more accurately represent the underlying trabecular bone. With this more accurate representation of the bone tissue, measurements made of that bone tissue will also be more accurate. Thus, DEI makes more efficient use of dose. Though it is possible to generate more accurate assessment of trabecular structure with high dose micro-CT, these findings suggest that it would not be possible to match DEI's contrast and resolution for a given dose, energy and detector resolution.

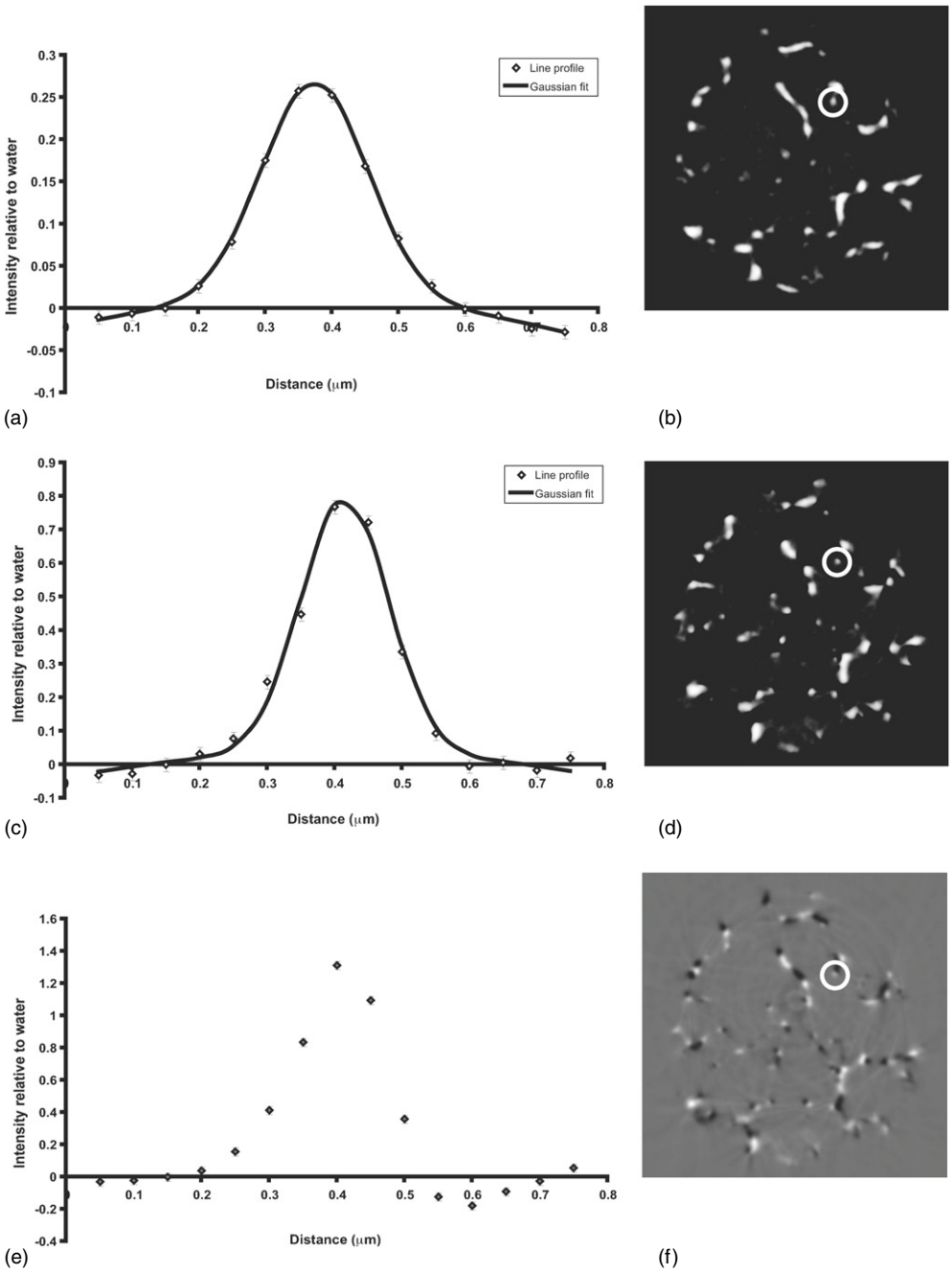

Figure 5. Example line profiles from small features in the trabecular bone slice images. Plots (a), (c) and (e) are from the SRCT slice, the apparent absorption DECT slice and the refraction DECT slice, respectively. The Gaussian fit is shown for the SR (a) and apparent absorption profile (c). The slice image is shown in (b), (d) and (f) for SRCT, apparent absorption DECT and refraction DECT images, respectively, with the trabecular feature from the line profile encircled.

The CNR results may seem to be contradictory to the findings of Dilmanian *et al* (2000) where apparent absorption DECT was shown not to have contrast gains over SRCT. In their experiment, they imaged an acrylic cylinder with an angularly cut drill hole that was filled with olive oil. Olive oil is far less scattering than bone so we should expect there to be very little extinction contrast gain. So what little was gained with extinction contrast was lost through the addition of noise caused by adding two images together to form the apparent absorption DECT image.

The rejection of scatter that leads to additional contrast in the apparent absorption images leads to a reduction in contrast in the refraction image. The large amount of USAXS in bone means that the refraction image results must be considered qualitatively rather than quantitatively, which limits the usefulness of the results. What can be inferred from the data is whether the index of refraction is increasing, decreasing or remaining the same along the vertical direction within the voxel. If one assumes there is no variation in the index of refraction within materials (i.e. the entire region is composed of either n_{bone} or n_{water}), then a black or white pixel means there is an interface between materials within that voxel. If we assume that the trabecular bone is uniform density bone interspersed with, in this case, water, then a black pixel in the refraction DECT slice image means that there is an interface between water and bone in which the water region of that volume is above the bone region of that volume.

6. Conclusions

The findings presented here, when combined with the previous findings in DECT of soft tissue features (Fiedler *et al* 2004, Keyriläinen *et al* 2008), show that DECT has enhanced contrast over SRCT for both soft tissue features and bone; the CNR gains that are seen over SRCT for soft tissue do not come at the expense of image quality for features within the bone. Thus DECT will prove to be a useful tool for imaging applications in which high contrast and high resolution are simultaneously required for both soft tissue features and bone.

Acknowledgments

Thanks to the Gift of Hope Organ and Tissue Donor Network for providing the samples. The research was supported by an NCSU FRPD grant, by the Department of the Army grant DAMD170110811, by the US Department of Energy contract no DE-AC02-98CH10886, by NIH grants R01 AR48292 and AR039239 and by the Brookhaven National Laboratory LDRD grant 05-057.

References

Arfelli F *et al* 2000 Mammography with synchrotron radiation: phase-detection techniques *Radiology* **215** 286–93

Bravin A 2003 Exploiting the x-ray refraction contrast with an analyser: the state of the art *J. Phys. D: Appl. Phys.* **36** A24–9

Bravin A *et al* 2007 High-resolution CT by diffraction-enhanced x-ray imaging: mapping of breast tissue samples and comparison with their histo-pathology *Phys. Med. Biol.* **52** 2197–211

Chapman D, Thomlinson W, Arfelli F, Gmür N, Zhong Z, Menk R, Johnston R E, Washburn D, Pisano E and Sayers D 1996 Mammography imaging studies using a Laue crystal analyzer *Rev. Sci. Instrum.* **67** (published on CD-ROM)

Chapman D, Thomlinson W, Johnston R E, Washburn D, Pisano E, Gmur N, Zhong Z, Menk R, Arfelli F and Sayers D 1997 Diffraction enhanced x-ray imaging *Phys. Med. Biol.* **42** 2015–25

Coan P, Pagot E, Fiedler S, Cloetens P, Baruchel J and Bravin A 2005 Phase-contrast x-ray imaging combining free space propagation and Bragg diffraction *J. Synchrotron Radiat.* **12** 241–5

Connor D, Dilmanian F A, Parham C, Kao T and Zhong Z 2007 Energy and dose considerations for diffraction enhanced CT in small animal studies *Medical Imaging 2007: Physics of Medical Imaging; Proc. SPIE* **6510** 65103K

Connor D M, Benveniste H, Dilmanian F A, Kritzer M F, Miller L M and Zhong Z 2009 Computed tomography of amyloid plaques in a mouse model of Alzheimer's disease using diffraction enhanced imaging *Neuroimage* **46** 908–14

Connor D M, Sayers D, Sumner D R and Zhong Z 2005 Identification of fatigue damage in cortical bone by diffraction enhanced imaging *Nucl. Instrum. Methods Phys. Res.* A **548** 234–9

Connor D M, Sayers D, Sumner D R and Zhong Z 2006 Diffraction enhanced imaging of controlled defects within bone, including bone-metal gaps *Phys. Med. Biol.* **51** 3283–300

Davis T J 1996 X-ray diffraction imaging using perfect crystals *J. X-Ray Sci. Technol.* **6** 317–42

Davis T J, Gureyev T E, Gao D, Stevenson A W and Wilkins S W 1995 X-ray image-contrast from a simple phase object *Phys. Rev. Lett.* **74** 3173–6

Dilmanian F A, Zhong Z, Ren B, Wu X Y, Chapman L D, Orion I and Thomlinson W C 2000 Computed tomography of x-ray index of refraction using the diffraction enhanced imaging method *Phys. Med. Biol.* **45** 933–46

Fiedler S, Bravin A, Keyrilainen J, Fernandez M, Suortti P, Thomlinson W, Tenhunen M, Virkkunen P and Karjalainen-Lindsberg M L 2004 Imaging lobular breast carcinoma: comparison of synchrotron radiation DEI-CT technique with clinical CT, mammography and histology *Phys. Med. Biol.* **49** 175–88

Forster E, Goetz K and Zaumseil P 1980 Double crystal diffractometry for the characterization of targets for laser fusion experiments *Kristall Technik* **15** 937–45

Gang L, Chen Z H, Wu Z Y, Ando M, Lin P, Wang J Y and Jiang X M 2004 Image quality dependence on thickness of sliced rat kidney taken by a simplest DEI construction *Nucl. Instrum. Methods Phys. Res.* A **548** 200–6

Hasnah M O, Parham C, Pisano E D, Zhong Z, Oltulu O and Chapman D 2005 Mass density images from the diffraction enhanced imaging technique *Med. Phys.* **32** 549–52

Hasnah M O, Zhong Z, Oltulu O, Pisano E, Johnston R E, Sayers D, Thomlinson W and Chapman D 2002 Diffraction enhanced imaging contrast mechanisms in breast cancer specimens *Med. Phys.* **29** 2216–21

Ingal V N and Beliaevskaya E A 1997 Phase dispersion introscopy *Surf. Invest.* **12** 441–50

Keaveny T M, Morgan E F, Niebur G L and Yeh O C 2001 Biomechanics of trabecular bone *Annu. Rev. Biomed. Eng.* **3** 307–33

Keyriläinen J *et al* 2008 Toward high-contrast breast CT at low radiation dose *Radiology* **249** 321–7

Kiss M Z, Sayers D E, Zhong Z, Parham C and Pisano E D 2004 Improved image contrast of calcifications in breast tissue specimens using diffraction enhanced imaging *Phys. Med. Biol.* **49** 3427–39

Kothari M, Keaveny T M, Lin J C, Newitt D C, Genant H K and Majumdar S 1998 Impact of spatial resolution on the prediction of trabecular architecture parameters *Bone* **22** 437–43

Li J, Zhong Z, Lidtke R, Kuettner K E, Peterfy C, Aliyeva E and Muehlemanll C 2004 Radiography of soft tissue of the foot and ankle with diffraction enhanced imaging *J. Am. Podiatr. Med. Assoc.* **94** 315–22

Link T M, Majumdar S, Grampp S, Guglielmi G, Van Kuijk C, Imhof H, Glueer C and Adams J E 1999 Imaging of trabecular bone structure in osteoporosis *Eur. Radiol.* **9** 1781–8

Majumdar S, Issever A S, Burghardt A, Lotz J, Arfelli F, Rigon L, Heitner G and Menk R H 2004 Diffraction enhanced imaging of articular cartilage and comparison with micro-computed tomography of the underlying bone structure *Eur. Radiol.* **14** 1440–8

Mannan K A *et al* 2004 Synchrotron supported DEI/KES of a brain tumor in an animal model: the search for a microimaging modality *Nucl. Instrum. Methods Phys. Res.* A **548** 106–10

Mollenhauer J, Aurich M E, Zhong Z, Muehleman C, Cole C C, Hasnah M, Oltulu O, Kuettner K E, Margulis A and Chapman L D 2002 Diffraction-enhanced x-ray imaging of articular cartilage *Osteoarthritis Cartilage* **10** 163–71

Muehleman C, Chapman L D, Kuettner K E, Rieff J, Mollenhauer J A, Massuda K and Zhong Z 2003 Radiography of rabbit articular cartilage with diffraction-enhanced imaging *Anat. Rec.* A **272** 392–7

Muehleman C *et al* 2004a X-ray detection of structural orientation in human articular cartilage *Osteoarthritis Cartilage* **12** 97–105

Muehleman C, Sumner D R and Zhong Z 2004b Refraction effects of diffraction enhanced radiographic imaging—a new look at bone *J. Am. Podiatr. Med. Assoc.* **94** 453–5

Muehleman C, Whiteside M, Zhong Z, Mollenhauer J, Aurich M, Kuettner K E and Chapman L D 2002 Diffraction enhanced imaging for articular cartilage *Biophys. J.* **82** 470A

Muller R, Hahn M, Vogel M, Delling G and Ruegsegger P 1996 Morphometric analysis of noninvasively assessed bone biopsies: comparison of high-resolution computed tomography and histologic sections *Bone* **18** 215–20

Oltulu O, Zhong Z, Hasnah M, Wernick M N and Chapman D 2003 Extraction of extinction, refraction and absorption properties in diffraction enhanced imaging *J. Phys. D: Appl. Phys.* **36** 2152–6

Pagot E, Cloetens P, Fiedler S, Bravin A, Coan P, Baruchel J, Hartwig J and Thomlinson W 2003 A method to extract quantitative information in analyzer-based x-ray phase contrast imaging *Appl. Phys. Lett.* **82** 3421–3

Pavlov K M, Gureyev T E, Paganin D, Nesterets Y I, Morgan M J and Lewis R A 2004 Linear systems with slowly varying transfer functions and their application to x-ray phase-contrast imaging *J. Phys. D: Appl. Phys.* **37** 2746–50

Pisano E D *et al* 2000 Human breast cancer specimens: diffraction-enhanced imaging with histologic correlation—improved conspicuity of lesion detail compared with digital radiography *Radiology* **214** 895–901

Rivers M 1998 Tutorial introduction to x-ray computed microtomography data processing http://www-fp.mcs.anl.gov/xray-cmt/rivers/tutorial.html (accessed 13 August 2003)

Rocha H S, Lopes R T, Valiante P M, Tirao G, Mazzaro I, Honnicke M G, Cusatis C and Giles C 2004 Diagnosis of thyroid multinodular goiter using diffraction-enhanced imaging *Nucl. Instrum. Methods Phys. Res.* A **548** 175–80

Ulrich D, Van Rietbergen B, Laib A and Ruegsegger P 1999 The ability of three-dimensional structural indices to reflect mechanical aspects of trabecular bone *Bone* **25** 55–60

Wagner A *et al* 2004 Options and limitations of joint cartilage imaging: DEI in comparison to MRI and sonography *Nucl. Instrum. Methods Phys. Res.* A **548** 47–53

Wagner A *et al* 2006 Qualitative evaluation of titanium implant integration into bone by diffraction enhanced imaging *Phys. Med. Biol.* **51** 1313–24

Wernick M N, Wirjadi O, Chapman D, Zhong Z, Galatsanos N P, Yang Y Y, Brankov J G, Oltulu O, Anastasio M A and Muehleman C 2003 Multiple-image radiography *Phys. Med. Biol.* **48** 3875–95

Zachariasen W H 1945 *Theory of X-Ray Diffraction in Crystals* (New York: Wiley)

Zhong Z, Thomlinson W, Chapman D and Sayers D 2000 Implementation of diffraction-enhanced imaging experiments: at the NSLS and APS *Nucl. Instrum. Methods Phys. Res.* A **450** 556–67